REFINEMENT OF A SECOND MOMENT CLOSURE BY ELLIPTIC BLENDING MODEL AND ITS APPLICATION TO ROTATING TURBULENT CHANNEL FLOWS

Jong Keun Shin
Department of Automotive Engineering, Donghae University,
119, Jiheung-dong, Donghae, Kangwondo 240-713, Korea
jkshin@donghae.ac.kr

Kun Ho Chun, Young Don Choi
Department of Mechanical Engineering, Korea University,
1, Anam-dong, Sungbuk-ku, Seoul 136-701, Korea
khchun@korea.ac.kr, ydchoi@korea.ac.kr

ABSTRACT

This paper describes further developments of a near-wall second moment turbulence closure of Manceau and Hanjalic(2002), and its application to the imposed system rotation. To refine the model, called "the elliptic blending model", an inhomogeneity correction is added to the near-wall redistribution term. Also, another approach to modelling the near-wall limiting redistribution is employed for the general complex geometries, which frequently appears in industrial applications. Concerning the homogeneous redistribution, the model of Speziale-Sarkar-Gatski(SSG) is replaced by a Launder-Tselepidakis non-linear model. The present refined model is tested by direct comparison with the DNS to validate the performance of predictions.

INTRODUCTION

In order to make more convenient use of the second moment turbulent closures, Durbin(1993) proposed the elliptic relaxation method(ERM), which can be directly extended to the models down to the wall with acceptable coarse grids. However, the ERM of Durbin includes six additional equations inducing the numerical instability due to their boundary conditions, which impedes its spreading into the industry. In order to make up a weak point of the ERM, Manceau and Hanjalic(2002, hereafter denoted by MH) suggest another approach, which is based on a blending of near-wall and far-from the wall forms of pressure redistribution tensor, called "the elliptic blending model(EBM)", the ellipticity being preserved by solving an elliptic blending function. The model guarantees the main feature of Durbin's elliptic relaxation second moment model but involves only one scalar elliptic equation. Also, the model has the possibility of application on industry since this approach offers a reasonable compromise between simplicity and consistency with physics. Despite the above mentioned merits, the predictions due to MH-EBM may not provide satisfactory results in the complex flows such as imposed system rotation, since the model reproduces under-estimated wall-normal Reynolds stress distribution even in simple channel flows.

The present contribution describes further developments of a near-wall second moment closure due to the refinement of MH-EBM for convenient industrial applications and its application to the imposed system rotation to test the performance of the model. The refinement is achieved by repairing the redistribution model and the dissipation tensor. Two different, but orthogonal rotation vectors coincident with the Cartesian coordinates have been imposed on plane channel cases, which are related to spanwise and streamwise rotating flows.

MATHEMATICAL MODELS

The original elliptic blending model

The stress transport model in an incompressible flow can be written as

$$\frac{D\overline{u_iu_j}}{Dt} = P_{ij} + F_{ij} + D^{\nu}_{ij} + D^{T}_{ij} + \Phi^{*}_{ij} - \epsilon_{ij}. \qquad (1)$$

The terms on the right-hand side of Eq. (1) are identified as generation due to mean shear(P_{ij}) and system rotation(F_{ij}), viscous diffusion(D^{ν}_{ij}) and turbulent diffusion(D^{T}_{ij}) associated with velocity, redistribution(Φ^{*}_{ij}) and dissipation(ϵ_{ij}), respectively. To impose the limiting behaviour of the fluctuating quantities of Reynolds stresses, Durbin(1993) proposed the ERM as

$$\Phi^{*}_{ij} - \epsilon_{ij} = kf_{ij} - \frac{\overline{u_iu_j}}{k}\epsilon. \qquad (2)$$

In the above model, f_{ij} is obtained from the elliptic relaxation equation as

$$f_{ij} - L^2\nabla^2 f_{ij} = \frac{1}{k}\left(\Phi^{h}_{ij} - \frac{2}{3}\epsilon\delta_{ij} + \frac{\overline{u_iu_j}}{k}\epsilon\right). \qquad (3)$$

Also, Durbin(1993) suggested the wall boundary conditions of f_{ij} equations to reproduce the wall limiting behaviour of $\Phi^{*}_{ij} - \epsilon_{ij}$. However, because the six additional equations for f_{ij} induce numerical stiffness by the imposed boundary conditions, MH proposed a simpler model preserving the main features of the ERM. The proposal of MH is to

model the redistribution term by

$$\Phi_{ij}^{*} = (1 - k\alpha)\Phi_{ij}^{w} + k\alpha\Phi_{ij}^{h}, \quad (4)$$

and the dissipation by

$$\epsilon_{ij} = (1 - A\,k\alpha)\frac{\overline{u_i u_j}}{k}\epsilon + A\,k\alpha\frac{2}{3}\epsilon\delta_{ij}, \quad (5)$$

where, k is turbulent kinetic energy and A is the stress flatness invariant suggested by Lumley (1978). And, the ellipticity of the model is preserved by solving an elliptic differential equation as

$$\alpha - L^2\nabla^2\alpha = \frac{1}{\epsilon T}, \quad (6)$$

with the boundary conditions $\alpha = 0$ at the wall. For the reproduction of the limiting wall behaviour of Φ_{ij}^{w}, MH suggested the near-wall redistribution term and a new wall-normal vector concept as

$$\Phi_{ij}^{w} = -5\frac{\epsilon}{k}\left(\overline{u_i u_k}n_j n_k + \overline{u_j u_k}n_i n_k - \frac{1}{2}\overline{u_k u_l}n_k n_l(n_i n_j + \delta_{ij})\right) \quad (7)$$

$$\mathbf{n} = \frac{\nabla\alpha}{|\nabla\alpha|}. \quad (8)$$

Concerning the quasi-homogeneous model Φ_{ij}^{h} $(= \Phi_{ij}^{slow} + \Phi_{ij}^{rapid})$, MH adopted the Speziale, Sarkar and Gatski(SSG, 1991) model with some modification in the coefficient.

In Eq. (6), the time scale T and length scale L are bounded by Kolmogorov scale as the ERM of Durbin(1993).

Refinement of the elliptic blending model

Obviously, it is true that MH-EBM is proposed to meet industrial needs for a simple and convenient model, while still preserving the elliptic relaxation concept and satisfying the near-wall limiting behaviour. However, because the wall-normal vector of MH-EBM is not tested by any internal flows, it is necessary to examine the validation of the wall-normal vector in a three-dimensional flow. Although the profiles of mean velocity and Reynolds shear stress in the computations of channel flow due to MH-EBM are globally well predicted, the profile of Reynolds normal stress is not fully satisfactory in comparison with that of the direct numerical simulation(DNS) data. Also, in spanwise rotating channel flows, MH-EBM can induce the numerical instability in high rotation rate, which may be caused by the under-estimated wall-normal stress $\overline{u_2 u_2}$ profile. In order for the model to be used for the industrial flows including the imposed system rotation, the redistribution model in this study is revised to meet universal constraints as

$$\Phi_{ij}^{*} = (1 - k\alpha)(\Phi_{ij}^{w} + \Phi_{ij}^{inh}) + k\alpha\Phi_{ij}^{h}, \quad (9)$$

$$\Phi_{ij}^{w} = 5\left(\nu\frac{\overline{u_l u_n}}{k}\frac{\partial\sqrt{k}}{\partial x_l}\frac{\partial\sqrt{k}}{\partial x_n}\delta_{ij} - \frac{3}{2}\nu\frac{\overline{u_i u_l}}{k}\frac{\partial\sqrt{k}}{\partial x_j}\frac{\partial\sqrt{k}}{\partial x_l} - \frac{3}{2}\nu\frac{\overline{u_l u_j}}{k}\frac{\partial\sqrt{k}}{\partial x_i}\frac{\partial\sqrt{k}}{\partial x_l}\right) \quad (10)$$

$$\Phi_{ij}^{inh} = C_{\Phi}\frac{\epsilon}{k^2}\overline{u_l u_n}\left(\overline{u_n u_k}d_k^A\delta_{ij} - \frac{3}{2}\overline{u_i u_n}d_j^A - \frac{3}{2}\overline{u_j u_n}d_i^A\right)d_l^A \quad (11)$$

$$d_i^A = \frac{N_i^A}{0.5 + (N_k^A N_k^A)^{0.5}}, \quad N_i^A = \frac{\partial(k^{1.5}A^{0.5}/\epsilon)}{\partial x_i} \quad (12)$$

with the elliptic blending function α suggested by MH. That is, to apply the model to complex geometries, we employed another near-wall redistribution approach Φ_{ij}^{w} on the satisfaction of wall limiting conditions. And, in order to sensitize the model to strong inhomogeneity in the buffer region of wall shear flow, we adopted the indicator of length-scale gradient direction d_i^A on the inhomogeneity redistribution model Φ_{ij}^{inh} which is introduced by Craft(1998). If the length-scale gradients are large, the value of d_i^A is close to unity, while it becomes negligible in the regions of small inhomogeneity. Consequently, the revised near-wall redistribution model considers the satisfaction of wall limiting behaviour and inhomogeneity effects induced in the buffer region.

To decide the coefficient C_{Φ} of the inhomogeneous redistribution model, an *a priori* test has been performed with the DNS database for a channel flow at $Re_{\tau} = 590$, and then a numerical stability test is carried out to give the confidence of the present model by the channel flow. These test results suggest that $C_{\Phi} = 5.0$.

Fig. 1 shows the redistribution model profiles obtained from the *a priori* test. It can be observed that the revised present model overestimates the redistribution of Φ_{12}^{*}, but predicts correctly Φ_{11}^{*} in comparison with the DNS data.

In order to enhance the ability of prediction in the high Reynolds number region, we employed the non-linear slow term and the cubic quasi-isotropic rapid model of Launder and Tselepidakis(1991), which can be expressed as

$$\begin{aligned}\Phi_{ij}^{h} = &-2(C_1 + 1)\epsilon b_{ij} - 4C_1'\epsilon\left(b_{ik}b_{kj} - \frac{1}{3}II_b\delta_{ij}\right)\\ &+ \frac{4}{5}kS_{ij} + 1.2k\left(b_{ik}S_{jk} + b_{jk}S_{ik} - \frac{2}{3}b_{kl}S_{kl}\delta_{ij}\right)\\ &+ \frac{26}{15}k(b_{ik}W_{jk} + b_{jk}W_{ik}) + \frac{4}{5}k(b_{ik}b_{kl}W_{jl} + b_{jk}b_{kl}W_{il})\\ &+ \frac{4}{5}k(b_{ik}b_{kl}S_{jl} + b_{jk}b_{kl}S_{il} - 2b_{ik}S_{kl}b_{lj} - 3b_{kl}S_{kl}b_{ij})\\ &+ C_2k\{16II_b(b_{ik}W_{jk} + b_{jk}W_{ik})\\ &+ 48(b_{ik}b_{kl}W_{lm}b_{mj} + b_{jk}b_{kl}W_{lm}b_{ml})\}, \end{aligned} \quad (13)$$

where

$$S_{ij} = \frac{1}{2}\left(\frac{\partial U_i}{\partial x_j} + \frac{\partial U_j}{\partial x_i}\right), \quad (14)$$

$$W_{ij} = \frac{1}{2}\left(\frac{\partial U_i}{\partial x_j} - \frac{\partial U_j}{\partial x_i}\right) + e_{mji}\Omega_m \quad (15)$$

are the mean rate of strain and absolute mean vorticity tensor. The anisotropy tensor and its invariant are defined as

$$b_{ij} = \frac{1}{2}a_{ij} = \frac{\overline{u_i u_j}}{2k} - \frac{1}{3}\delta_{ij}, \quad (16)$$

$$II_b = b_{ij}b_{ji}, \quad (17)$$

$$A = 1 - \frac{9}{8}(a_{ij}a_{ji} - a_{ij}a_{jk}a_{ki}). \quad (18)$$

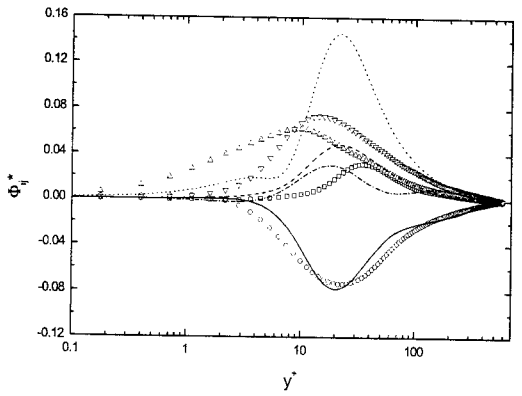

Fig. 1 *A priori* test in a channel flow for redistribution model at $Re_\tau = 590$. symbols : DNS, lines : models (○, — Φ^*_{11}; □, -·- Φ^*_{22}; △, --- Φ^*_{33}; ▽, ····· Φ^*_{12})

The adopted model coefficients in the present study are $C_1 = 3.1\,(A\min(4II_b, 0.6))^{1/2}$, $C_1' = 0.2C_1$ and $C_2 = \min(0.6, A)$. Note that the coefficient C_1' has been set to 0.2 instead of -1.2, which leads to better predictions on the profiles of wall-normal Reynolds stress mainly in the core region. Also, we replace the dissipation model through the calibration processes to enhance the distribution of streamwise Reynolds stress in the buffer region.

$$\epsilon_{ij} = (1-\sqrt{A}\,k\alpha)\frac{\overline{u_iu_j}}{k}\epsilon + \sqrt{A}\,k\alpha\frac{2}{3}\epsilon\delta_{ij} \qquad (19)$$

The unclosed diffusion term in Eq. (1) is modelled via the standard gradient transport hypothesis as

$$D^T_{ij} = \frac{\partial}{\partial x_l}\left(C_k\overline{u_lu_m}\,T\frac{\partial\overline{u_iu_j}}{\partial x_m}\right), \qquad (20)$$

with the coefficient $C_k = 0.22$.

In order to close the set of governing equations, the transport equation for ϵ is adopted from the ERM of Durbin(1993) as

$$\frac{D\epsilon}{Dt} = \frac{C^*_{\epsilon1}P_k - C_{\epsilon2}\epsilon}{T} + \frac{\partial}{\partial x_l}\left(C_\epsilon\overline{u_lu_m}\,T\frac{\partial\epsilon}{\partial x_m}\right) + \nu\frac{\partial^2\epsilon}{\partial x_k\partial x_k} \qquad (21)$$

where $C^*_{\epsilon1} = C_{\epsilon1}\,(1+0.1P_k/\epsilon)$ and the use of the time scale T is the only modifications of the standard high Reynolds number model equation. The coefficients appearing in the equation are chosen as $C_{\epsilon1} = 1.35$, $C_{\epsilon2} = 1.83$ and $C_\epsilon = 0.17$.

NUMERICAL TREATMENT

The Reynolds-averaged Navier Stokes equation (RANS) simulation using the present refined model has been performed for the fully developed non-rotating and rotating channel flows. The computations for channel flows are carried out with a simple finite-volume solver and the majority of the grids is laid in the low Reynolds number region ($y^+ \le 70$) while the first grid is located at $y^+ = 0.1$.

The Reynolds stresses and the mean velocities were set to 0 at the wall, and the wall dissipation rate was assigned to $\epsilon = 2\nu(\partial\sqrt{k}/\partial x_2)^2$.

RESULTS AND DISCUSSION

Non-rotating channel flows

Profiles of Reynolds stress in fully developed non-rotating channel flow are plotted in Fig. 2(a) compared to the DNS and MH-EBM. The fully developed non-rotating flow is performed to calibrate the present model at $Re_\tau = 590$. This figure shows that the anisotropy is globally well predicted. When compared to the MH-EBM, the distribution of $\overline{u_1u_1}$ in the wake region is not as well-captured, but its peak is better reproduced.

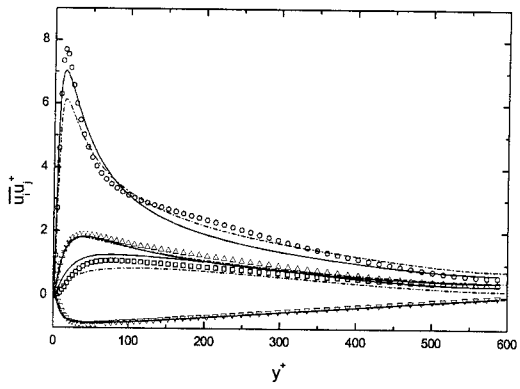

(a)

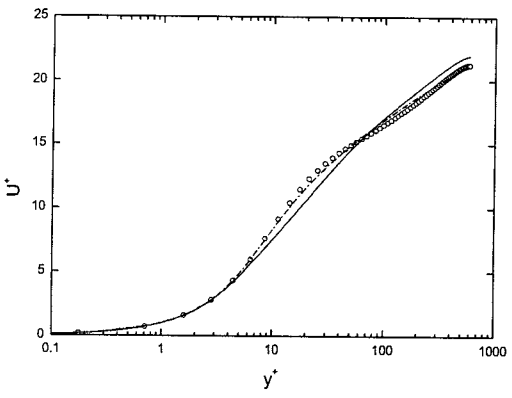

(b)

Fig. 2 Predicted flow behaviour in a non-rotating channel at $Re_\tau = 590$. symbols : DNS, — : present model, -·- : MH-EBM (a) Reynolds stress profiles. (○ $\overline{u_1u_1}$; □ $\overline{u_2u_2}$; △ $\overline{u_3u_3}$; ▽ $\overline{u_1u_2}$) (b) Mean velocity profiles.

The profile of $\overline{u_2u_2}$ is slightly over-estimated in the buffer region, but the profiles of $\overline{u_3u_3}$ and $\overline{u_1u_2}$ are similar and reasonably close to the DNS. It can be seen in Fig. 2(b) that the prediction of the mean velocity profile by MH-EBM is close to the DNS in comparison with the present model. This problem seems to be induced by the present near-wall redistribution model, which is introduced to consider the inhomogeneity effect in the buffer region, and we must remember the overestimated Φ_{12}^{*} profile in the *a priori* test. As will be seen later, however, the inhomogeneity term offers the potential for far more reliable predictions on the imposed system rotation.

In order to determine the present model coefficients, we computed the non-rotating channel flows. The model coefficients taken from this calibration procedure should not have been altered for the imposed system rotation flow.

Spanwise rotating channel flows

Coriolis and centrifugal forces arising from imposed system rotation can substantially alter the mean flow, the intensity and the structure of turbulence. Second moment closure is the most natural level of turbulence model closure to account for rotation, because this modelling approach approves the appearance of the exact production terms due to mean flow gradients and system rotation. Thus, in order to test the prediction ability of a second moment closure, it is natural to consider the rotating channel flow. A sketch of the computational domain is shown in Fig. 3, Cases SP and ST correspond to the rotation around spanwise and streamwise axes, respectively.

When the channel rotates about a spanwise axis, Coriolis forces stabilize the turbulent flow near the leading(suction) wall and augments the turbulence near the trailing(pressure) wall.

Fig. 4 shows the comparisons of turbulent rms velocity across the channel with the DNS data of Andersson and Kristoffersen(1995) in spanwise rotating channel flows. The rotation number Ro is defined using the channel width D, rotation rate Ω and the bulk mean velocity U_b. The predicted results are limited to the present refined model, because MH-EBM has failed to reproduce the DNS at high rotation due to a numerical instability. The present model predictions of the rms velocities in Fig. 4(a), which is related to Rotation number

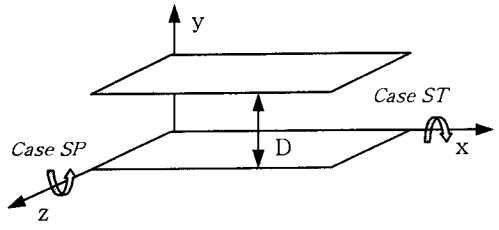

Fig. 3 Computational domain of rotating channel

$Ro = 0.1$, compare favorably with the DNS on the pressure side, but some discrepancies are observed on the suction side. However, as shown in Fig. 4(b), the rms velocities at the Rotation number $Ro = 0.5$ are well reproduced with the inclination of relaminarization on the suction side. The continuous augmentation of wall-normal intensity on the pressure side with increased Rotation number is well captured by the present model. Fig. 4(c) shows the predicted mean velocity profiles across the channel. The position of maximum mean velocity is shifted towards the suction side of the channel and the profiles exhibit the characteristic asymmetry introduced by the imposed system rotation which increases with the rotation number. The model prediction due to $Ro = 0.5$ compares well with the DNS data. The normalized friction velocities on the unstable and stable sides are compared with the DNS of Andersson and Kristoffersen(1995) and the experimental data of Johnston et al.(1972) as shown in Fig. 5. The present model and the DNS are in good agreement on the both unstable and stable sides. But, a more significant difference can be observed on the stable side in comparison with experimental data. That is, the predictions do not exhibit the distinct drop for $Ro > 0.1$ as indicated by the experiments of Johnston et al.(1972).

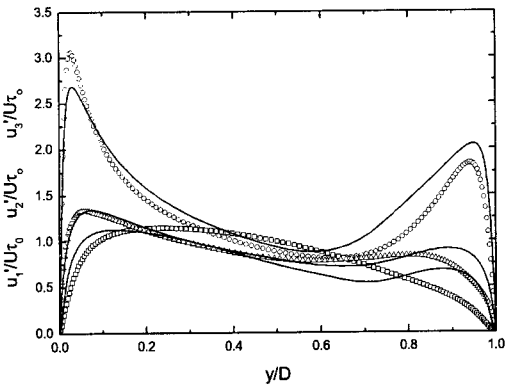

(a)

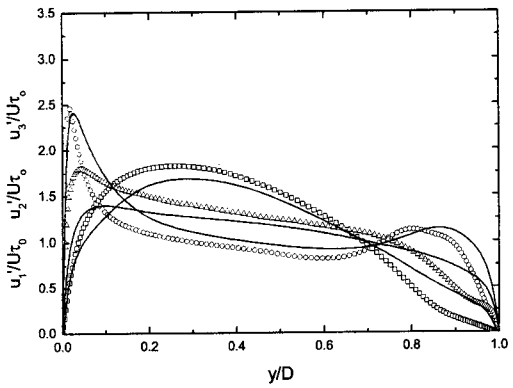

(b)

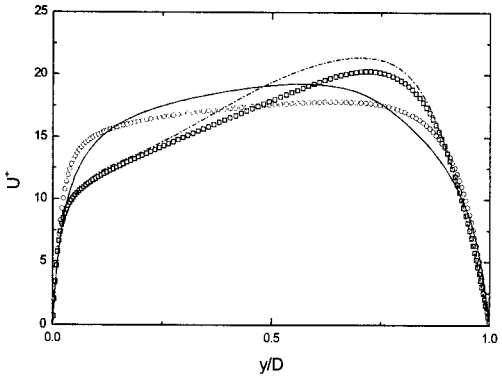

(c)

Fig. 4 Summary of predicted flow behaviour in a spanwise rotating channel at $Re_\tau = 194$. symbols : DNS (○ $\overline{u_1u_1}$; □ $\overline{u_2u_2}$; △ $\overline{u_3u_3}$), lines : present model (a) rms velocity fluctuations at $Ro = 0.1$. (b) rms velocity fluctuations at $Ro = 0.5$. (c) Mean velocity profiles. symbols : DNS, lines : present model (○, — $Ro = 0.1$; □, -·- $Ro = 0.5$)

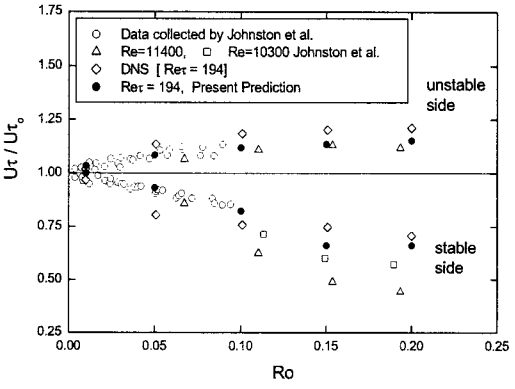

Fig. 5 Normalized friction velocities on the two sides of the channel.

It is noted that, in the calculations with the present model, a rotating source term in the ϵ equation, which is frequently added in other elliptic relaxation equation models to reproduce the rotation effects(Wizman et al. 1996), is not used. Since the additional rotating source term is purely empirical, we think that the use of the term can induce the unphysical phenomena on the complex industrial applications.

Streamwise rotating channel flows

The streamwise rotating channel is a challenging flow field for a second moment turbulence closure, because, in comparison with the spanwise rotating, all six Reynolds components are non-zero. Thus, with the simple flow field relatively, we can decide whether a new second moment closure reproduces all Reynolds stress components satisfactorily or

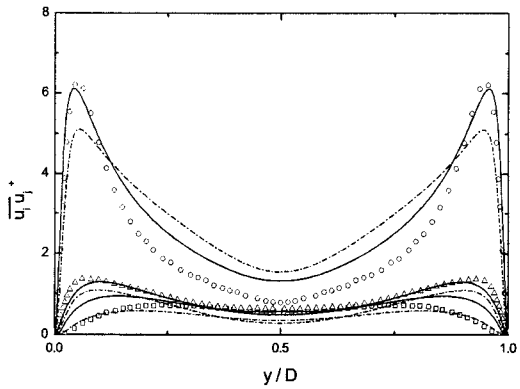

(a)

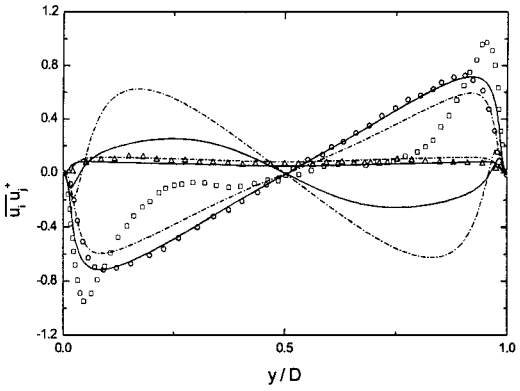

(b)

Fig. 6 Predicted flow behaviour in a streamwise rotating channel at $Re_\tau = 150$ and $Ro_\tau = 7.5$. symbols : DNS, — : present model, -·- : MH-EBM (a) Normal stress profiles. (○ $\overline{u_1u_1}$; □ $\overline{u_2u_2}$; △ $\overline{u_3u_3}$) (b) Shear stress profiles. (○ $\overline{u_1u_2}$; □ $\overline{u_1u_3}$; △ $\overline{u_2u_3}$)

not. In case a fully developed channel flow is imposed by streamwise rotation, all normal stresses and $\overline{u_2u_3}$ are symmetric about the centerline. In contrast to those cases, $\overline{u_1u_2}$ and $\overline{u_1u_3}$ are antisymmetric about the centerline. From the mean momentum equations for a fully developed streamwise rotation channel(Oberlack et al, 1999), we can derive that the distribution of $\overline{u_1u_2}$ varies linearly across the channel, because the pressure-gradient in the streamwise direction is constant. It should be noted that the profiles of $\overline{u_1u_2}$ and $\overline{u_2u_3}$ influence the streamwise and spanwise mean velocities respectively. Although $\overline{u_1u_3}$ is not dependent directly on a mean momentum equation in a fully developed streamwise rotating flow, the components obviously exist due to the rotation.

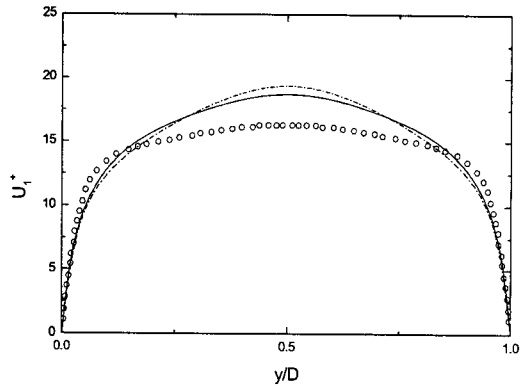

(a)

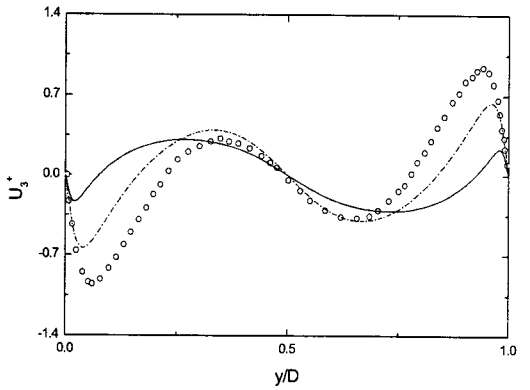

(b)

Fig. 7 Mean velocity profiles in a streamwise rotating channel at $Re_\tau = 150$ and $Ro_\tau = 7.5$. symbols : DNS, — : present model, -·- : MH-EBM. (a) Streamwise mean velocity (b) Spanwise mean velocity.

Fig. 6(a) shows the Reynolds stress profiles across the streamwise rotating channel. The predicted rotation number is $Ro_\tau = 7.5$, which is based on the channel width D, rotation rate Ω and the friction velocity of the non-rotating case $U_{\tau o}$. It is interesting to note that the overall property of DNS(El-Samni and Kasagi, 2001) is quite well represented by the present refined model and MH-EBM. The profile of $\overline{u_3u_3}$ is fairly well reproduced but the profile of $\overline{u_2u_2}$ is over-estimated in the wall region by the present model. MH-EBM under-estimates the profile of $\overline{u_2u_2}$ in the channel core region as the case of non-rotating flow. It can be seen in Fig. 6(b) that, from shear stresses, $\overline{u_1u_2}$ profile based on the present model and $\overline{u_2u_3}$ profile based on MH-EBM are obtained with reasonable agreement compared to the DNS of El-Samni and Kasagi(2001). Although an almost constant component $\overline{u_2u_3}$ is obtained from both models in the center region of the flow as predicted by the DNS, the distribution due to the present model is under-estimated in comparison with the DNS and MH-EBM. The profiles of streamwise mean velocity due to the present model, which is only influenced by shear stress $\overline{u_1u_2}$ in the streamwise mean momentum equation, is close to the DNS in comparison with MH-EBM. In contrast to that case, as shown in Fig. 7(b), because the spanwise mean velocity is mainly influenced by component $\overline{u_2u_3}$, the spanwise velocity prediction due to MH-EBM is close to the DNS with superiority in component $\overline{u_2u_3}$ prediction. Refer to the component $\overline{u_1u_3}$, predictions by the models are not able to reproduce the proper trends of the DNS. The predicted $\overline{u_1u_3}$ profiles in the whole region except near the wall show the opposite result of that obtained by the DNS.

CONCLUSIONS

The appropriateness of the present second moment closure is examined by comparing the prediction results with the DNS data.

In the spanwise rotating channel flow, the present model catches very well the effects of Coriolis forces on the turbulent rms velocity profiles according to the rotation rate. Although the distributions of shear stress $\overline{u_1u_3}$ across the streamwise rotation channel are not satisfactory in comparison with the DNS, the remainder of computed results including normal stress profiles are globally well captured by both the present model and MH-EBM. Thus, the overall results presented in the present article are in resonable agreement with the DNS data, giving confidence the present model can be applied to more complex flows.

REFERENCES

Andersson, H.I. and Kristoffersen, R., 1995. in *Turbulent Shear Flows*, 9, 53-70

Craft, T.J. 1998. *Int. J. Heat and Fluid Flow*, 19, 541-548

Durbin, P.A., 1993. *J. Fluid Mech.*, 249, 465-498

El-Samni, O. A and Kasagi, N. 2000. *Proc. 37th National Heat Transfer Symposium*, Kobe, 559-510

Johnston, J.P., Hallen, R.M. and Lezius, D.K. 1972. *J. Fluid Mech.*, 56, 533-557

Launder, B.E. and Tselepidakis, D.P. 1991. *Proc. 8th symposium on turbulence Shear Flows*, Munich, Germany, 29-1

Lumley, J.L. 1978. *Adv. Appl. Mech.*, 18, 123

Manceau, R. and Hanjalic, K. 2002. *Phys. Fluids*, 14, 744-754

Moser, R.D., Kim, J. and Mansour, N.N. 1999. *Phys. Fluids*, 11, 943-945

Oberlack, M. Cabot, W. and Rogers, M.M. 1999. *In the 1st int. Symp. in Turbulence and Shear Flow Phenomena*, USA, 85-90

Speziale, C.G., Sarkar, S. and Gatski, T.B. 1991. *J. Fluid Mech.*, 227, 245-272

Wizman, V., Laurence, D., Kanniche, M., Durbin, P. and Demuren, A. 1996. *Int. J. Heat Fluid Flow*, 17, 255-266